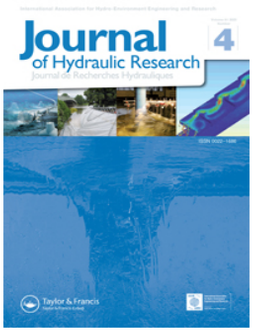

Journal of Hydraulic Research

ISSN: (Print) (Online) Journal homepage: https://www.tandfonline.com/loi/tjhr20

Analysis of the riverbed backscattered signal registered by ADCPs in different bedload transport conditions – field application

Slaven Conevski, Massimo Guerrero, Axel Winterscheid, Doreen Faltis, Colin D. Rennie & Nils Ruther

To cite this article: Slaven Conevski, Massimo Guerrero, Axel Winterscheid, Doreen Faltis, Colin D. Rennie & Nils Ruther (2023) Analysis of the riverbed backscattered signal registered by ADCPs in different bedload transport conditions – field application, Journal of Hydraulic Research, 61:4, 532-551, DOI: 10.1080/00221686.2023.2224276

To link to this article: https://doi.org/10.1080/00221686.2023.2224276

Published online: 18 Aug 2023.

Journal of Hydraulic Research Vol. 61, No. 4 (2023), pp. 532–551
https://doi.org/10.1080/00221686.2023.2224276

Research paper

Analysis of the riverbed backscattered signal registered by ADCPs in different bedload transport conditions – field application

SLAVEN CONEVSKI, Researcher/Adjunct Associate Professor, *Multiconsult Norway AS, Oslo; Department of Civil and Environmental Engineering, Norwegian University of Science and Technology, Trondheim, Norway*
Email: slaven.conevski@multiconsult.no; slaven.conevski@ntnu.no (author for correspondence)

MASSIMO GUERRERO, Senior Researcher/Assistant Professor, *Department of Civil, Chemical, Environmental, and Materials Engineering, University of Bologna, Bologna, Italy*
Email: massimo.guerrero@unibo.it

AXEL WINTERSCHEID, Group Leader/Research Engineer, *PhD, Federal Institute of Hydrology, Department of Fluvial Morphology, Sediment Dynamics and Management, Koblenz, Germany*
Email: winterscheid@bafg.de

DOREEN FALTIS, Engineer, *Federal Institute of Hydrology, Department of Fluvial Morphology, Sediment Dynamics and Management, Koblenz, Germany*
Email: Faltis@bafg.de

COLIN D. RENNIE, Professor, *Department of Civil Engineering, University of Ottawa, Ottawa, Canada*
Email: crennie@genie.uOttawa.ca

NILS RUTHER, *Technical University of Munich, Chair of Hydraulic Engineering, Munich, Germany*
Email: nils.ruether@tum.de

ABSTRACT
Acoustic Doppler current profilers (ADCP) were deployed to investigate the backscattering (BS) signal in three navigable rivers, in different bedload transport conditions. This study aims to demonstrate that the BS strength, as an additional variable to the apparent bedload velocity, improves the characterization of the bedload transport using ADCPs. The M9 –3 MHz and the vertical beam M9 – 0.5 MHz showed decline of the BS strength as the bedload intensity increased, whereas the RDI –1.2 MHz was relatively insensitive. The correlation between the median grain size and the BS strength for the 0.5 MHz was linear, for the 3 MHz the BS strength was attenuated in the active layer, and for 1.2 MHz, it revealed a parabolic distribution. Moreover, the analyses of the ADCP measured variables, using wavelet transformations and unsupervised machine learning, highlighted the importance of the spatial and temporal variance and transient nature of the bedload transport.

Keywords: Acoustic Doppler current profiler; backscattering strength; bedload apparent velocity; bedload transport; river morphology

1 Introduction

Sediment particles transported in flowing water, rolling or saltating, along a river bottom, are denoted as bedload (Bagnold, 1956). The riverbed surface consists of the sediment particles that are mobile, the bedload, as well as particles that are immobile, which collectively form the rough surface (Conevski et al., 2020b). The active bedload layer most often refers to the layer of mobile sediment at the riverbed (Church & Haschenburger, 2017). Compared to the suspended sediment transport, sediment particles transported in the water column, the bedload is characterized by much slower dynamics, but is crucial for shaping the river morphology. As such, a thorough understanding of bedload transport is essential for effective and sustainable sediment management, especially in large and heavily exploited, navigable rivers. Information about the bedload transport quantities and

Received 26 September 2022; accepted 6 June 2023/Open for discussion until 1 February 2024.

ISSN 0022-1686 print/ISSN 1814-2079 online
http://www.tandfonline.com

spatial distribution could significantly influence the dredging of the rivers, the definition of shipping routes, and the operation of hydraulic gates or any other man-made structures in the rivers.

The first step toward understanding bedload transport is data collection. Traditionally, the bedload dataset consists of bedload samples that represent the grain sizes of the sediment material present on the riverbed and bedload transport rates. Collecting bed surface samples is a labour-intensive but relatively simple routine. On the other hand, sampling bedload transport rates can be a notoriously hard and repetitive procedure (Bunte et al., 2007). The traditional direct methods for measuring bedload transport are typically intrusive techniques that collect the samples by direct contact with the riverbed. During the process, several issues contribute to large uncertainty in the sampling (Gaweesh & Van Rijn, 1994). The most advanced bedload samplers are the pressure difference samplers (Hubbell, 1964), which are placed on the riverbed manually and have a box or bag with a mesh to catch the sediment. The most frequent problems of these samplers are: (i) oversampling due to gouging of the bed surface during deployment, (ii) under-sampling due to perching on top of a large clast, such that transport goes underneath the sampler, (iii) under-sampling due to loss of material while raising the sampler, (iv) under-sampling due to clogging, and (v) under-sampling due to flow diversion (Brandstetter et al., 2012; Bunte et al., 2007). These measurements are non-continuous, often resulting in a statistically invalid estimation of the total bedload transport in a certain river reach. To reduce the uncertainty, a sufficient number of samples per position area is required and several positions per cross section must be conducted (Frings & Stefan, 2017; Gomez, 1991).

The above-mentioned difficulties have urged scientists and engineers to find alternative, easier, continuous, and less disruptive techniques. Very often dune tracking is an alternative method assuming that bedload transport rates can be estimated based on bedform migration (Claude et al., 2012; Leary & Buscombe, 2020; Simons et al., 1965). However, performing dune tracking requires frequent echo-sounding data as input to the analysis and is limited to river reaches with bedforms. Dune tracking provides estimates of the average bedload transport rate for an entire reach and for the time interval between two consecutive measurements. Another promising technique similar to dune tracking is acoustic mapping velocimetry (AMV), which is a technique that estimates bedload rates in rivers developing bed forms using multibeam scanning (Muste et al., 2016). However, these techniques do not give the local transport characteristics and fluctuations of transport over time.

On the other hand, the most promising surrogate techniques for bedload transport measurements in rivers are the hydro-acoustic techniques. The hydro-acoustic techniques are usually divided into passive and active acoustic methods. The passive acoustic techniques utilize geophones, hydrophones, or seismic arrays (Barrière et al., 2015; Geay et al., 2017; Hsu et al., 2011; Le Guern et al., 2021; Rickenmann et al., 2012, 2014; Roth et al., 2016).

Active acoustics techniques use the information from a returned echo signal (Urick, 1983). In riverine environments, the acoustic Doppler current profilers (ADCPs) are the most used monostatic active sonars. These are designed for measuring the water velocity and water discharge (Brumley et al., 1991; RDInstruments, 2011). However, in recent years many studies proved their ability to measure the suspended sediment load (Aleixo et al., 2020; Guerrero et al., 2013; Guerrero et al., 2016; Moore et al., 2013; Szupiany et al., 2019) using single and multifrequency, also enabling determination of the mean grain size (Guerrero et al., 2013; Moore et al., 2012). Besides the ADCPs, the acoustic backscatter is very often used to determine the suspended sediment concentration (SSC) at a point or short profiles, using high-frequency sonars such as LISST-ABS or AquaSCAT (Haun et al., 2015; Thorne & Hurther, 2014).

Bedload measurements using active acoustic systems work on the same principle as with the suspended sediment load, but the scattering process is more complex due to the multiphase scattering process (Conevski et al., 2020b; Darrell & Richardson, 2007). The bottom tracking (BT) velocity measured by ADCPs has demonstrated a reasonable matching with the bedload transport measured by traditional physical methods, both in stationary (Conevski et al., 2018; Conevski et al., 2020a; Rennie et al., 2002; Rennie & Villard, 2004) and moving boat conditions (Jamieson et al., 2011; Rennie & Church, 2010). Besides the field campaigns, several laboratory experiments have reported good correlations between the bedload velocity measured by video processing techniques and the BT velocity measured by different ADCPs (Conevski et al., 2019; Conevski et al., 2020b; Jamieson et al., 2008). Laboratory tests have also revealed a negative correlation between the corrected backscattering (BS) strength from the BT signal and the bedload concentration (Conevski et al., 2020b) measured by cameras, or the number of mobile particles per image in the gravel experiments, as well as different strengths of the vertical beam towards the sand and gravel bedload material (Conevski et al., 2020b). Another set of experiments advanced the bedload measurements and proved the possibility to profile the velocity and concentration of the bedload active layer by using bi-static active acoustic instruments (Blanckaert et al., 2017; Conevski et al., 2020c; Guta et al., 2022; Hurther & Thorne, 2011).

Other interesting field studies have demonstrated the impact of the BS strength on the apparent bedload velocity (Gaeuman & Jacobson, 2006) and the possibility to use the BS strength from the RDI 1.2 MHz slant beams to classify different bed materials in lakes (Shields, 2010).

1.1 *Motivation and objectives*

The estimation of the bedload transport rate using the ADCP apparent bedload velocity requires some assumptions related to the bedload concentration, active layer and grain size (Conevski et al., 2020a; Rennie & Villard, 2004). Often, the final determination of the transport rate relies on different empirical

and semiempirical equations to calculate these variables (Le Guern et al., 2021; Rennie & Villard, 2004). These assumptions introduce uncertainty that additionally complicates the transport rate calculation of the already highly variable motion of the bedload particles in time and space. The recent series of laboratory and field investigations have shown that the backscattering strength and the apparent bedload velocity have different behaviour toward different bedload materials (Conevski et al., 2020b; Rennie et al., 2017) and towards different bedload transport conditions (Conevski et al., 2020b). Consequently, post-processing of the BS signal and BT velocity in various locations could be rather complicated due to different bedload material, different roughness, biases, and ambient noise (Brumley et al., 1991; Conevski et al., 2020a; Conevski et al., 2020b). At the same time, the stationary ADCP measurements assume averaging of the relatively long time series, which generates information loss related to the temporal variability of the bedload (Parker, 2004). In an earlier field study (Conevski et al., 2020a), it was demonstrated that the different acoustic geometry and specific configuration of each ADCP influences the measurements of the bedload apparent velocity in different manners.

This field study is an extension of the work presented by Conevski et al. (2020a) and has two main experimental objectives: (i) to analyse the relations between the corrected BS strength and the transport intensity for different bedload particle size distributions (PSD); and (ii) to observe the temporal and spatial variations of both BT velocity and backscattering signal, by using techniques for decomposing the raw signal (e.g. wavelet transformations). The first goal has been initially shown in controlled laboratory settings (Conevski et al., 2020b; Conevski et al., 2020c) and partly in field conditions (Conevski et al., 2022). The present work aims to build upon these results and provide deeper insight into how to properly use the ADCP data. The second goal is partially examined in Conevski et al. (2022), but here, a deeper overview of the signal components is presented. In the end, unsupervised machine learning data classifiers are used to prove that the bedload characteristics, e.g. the grain size and transport intensity could be defined by using only the information delivered by the ADCPs. To engage these objectives, an M9 by Sontek and a RioGrande by RDI were deployed simultaneously, exploring weak to moderate bedload transport of sand to fine gravel material, in three different navigable rivers (Rhine, Elbe and Oder). Moreover, this study offers a significantly larger dataset from three different rivers covering different bedload transport conditions and PSDs.

2 Methodology

2.1 *Study sites*

The measurements were conducted in the three large rivers in Germany, the Rhine, Elbe and Oder, over a period of 6 years. The campaigns were part of regular sampling routines organized by the WSV (Waterways and Shipping Administration) and BfG (German Federal Institute of Hydrology) that collect sediment data during the entire year. Table 1 provides a list of the cross sections, locations, hydraulic conditions, and some bedload characteristics including the traditionally measured transport rate. Overall, there are 28 cross sections and more than 350 different positions. Note that data for some of the sandy cross sections from Elbe and Oder were also presented in Conevski et al. (2020a).

2.2 *Experimental set-up and procedure*

The experiments were organized as described in Conevski et al. (2020a). Two ADCPs were used, M9 by Sontek and RioGrande by RDI, mounted on small vessels on opposite sides of the survey ship (Fig. 1), ensuring that both are in a fixed position with minimum movements. The M9 operated with 3 MHz in all positions, mostly using the incoherent (IC) signal processing configuration, but sometimes it switched to pulse coherent SmartPulse HD (Conevski et al., 2020a). The RioGrande operated with 1.2 MHz, typical RDI broadband configuration (BB). The BT sampling rate ranged between 0.8 s and 2 s depending on the depth and the number of bins in the water profile. The pinging rate for the BT mode was always set to 1, and the rest of the commands remained at the default, as suggested by the manufacturers (RDI, 2015; Sontek, 2017). Note that in the previous studies (Conevski et al., 2020a; Conevski et al., 2020b) no significant changes were observed while using different signal processing and command configurations at the same frequency, regardless of the bedload transport conditions.

The BfG bedload sampler was operated by a crane on the side of the M9, at a distance of 10–15 m downstream, thus a possible interference was avoided (Fig. 1). On the opposite side of the ship, sometimes suspended sediment samples were collected using a pump sampler and filtering method. This data was used in the correction of the backscattering strength (Section 2.4).

The ADCPs were simultaneously and continuously measuring 10–30 min per each position along the cross-section. The bedload sampler was sampled two or three times per position, depending on the bedload transport conditions. Cameras were installed in the sampler structure (Fig. 2), to visualize the physical sampling and to understand if the sampler was correctly positioned and if there was blockage of the nozzle. If a problem was identified on the camera, the sample was not considered in the calculations, and in most cases, a new attempt was made at a slightly different location.

2.3 *Physical bedload sampling*

The bedload sampler used in these campaigns is developed by BfG, and apart from minor further developments, it has been in continuous use along German waterways for about 50 years. It is a pressure-difference sampler and was originally developed based on the Bed load Transport Meter Arnhem, BTMA

Table 1 Average hydraulic parameters given for the full cross-section

	Date	Pos. per CS	Location, name of the station	Distance from source (or the German border) km	Q (m^3 s^{-1})	H (m)	S ‰	D_{90} (D_{90grab}) (mm)	D_{50} (D_{50grab}) (mm)	$u*$ (m s^{-1})	$Q^m{}_s$ kg s^{-1} m^{-1}
ODER	17 May 2017	7	Neurüdnitz	656	748	2.59	0.15	1.7 (1.2)	0.6(0.5)	0.062	0.043
	18 May 2017	8	Hohenwutzen	662	721	3.12	0.15	1.8(3.5)	0.7(0.8)	0.068	0.076
ELBE down	27 March 2018	5	Neu Darchau	535.9	697	3.60	0.13	2.2 (3.3)	0.5 (0.8)	0.068	0.048
	28 March 2018	5	Wilkenstorf	516.2	691	2.56	0.11	2.5 (4.1)	0.7 (0.7)	0.052	0.044
	29 March 2018	5	Langendorf	501	702	3.27	0.13	2.6 (1.3)	0.5 (0.6)	0.065	0.088
	9 June 2021	5	Neu Darchau	535.9	489	3.10	0.12	3.1 (1.3)	0.6 (0.6)	/	0.035
	8 June 2021	5	Wilkenstorf	516.2	492	2.80	0.11	1.6 (10?)	0.6 (1.2)	/	0.055
	7 June 2021	5	Langendorf	501	504	3.17	0.13	3.2 (3.3)	0.8 (0.8)	/	0.025
ELBE up	28 May 2018	6	Barby	294	276	2.35	0.19	3.6 (2.8)	1.1 (0.9)	0.066	0.041
	29 May 2018	5	Saale downstream	291	323	2.22	0.20	3.4 (15?)	1.1 (1.9)	0.066	0.066
	29 May 2018	5	Saale upstream	290.6	246	2.14	0.20	3.1 (28.2)	1.1 (2.5)	0.065	0.055
	30 May 2018	6	Breitenhagen	287.8	221	1.91	0.19	3.5 (8.1)	1.1 (1.7)	0.060	0.042
	31 May 2018	5	Buckau	321	296	2.30	0.20	2.8 (2)	0.9 (0.8)	0.067	0.017
Middle Rheine	23 November 2020	9	Nierstein	483.5	820	3.98	0.09	4.7 (17.7)	9.3 (4.6)	0.058	0.005
	24 November 2020	10	Laubenheim	493.6	796	3.06	0.09	4.5 (35.5)	9.6 (6.9)	0.051	0.016
	25 25 November 2020	11	Mainz	498.3	903	3.11	0.09	1.3 (21.2)	4.0 (2.9)	0.051	0.006
	26 November 2020	12	Niederwalluf	508	925	3	0.09	1.4 (40.1)	4.2 (5.8)	0.050	0.004
	30 November 2020	9	Eltville	511.4	840	2.67	0.09	2.1 (39.9)	6.5 (7.4)	0.047	0.002
	1 December 2020	11	Oestrich	517.7	845	2.4	0.09	2.9 (35.5)	8.9 (7.5)	0.045	0.002
	2 December 2020	10	Bingen	528.8	861	2.06	0.09	1.3 (39.9)	5.8 (5.1)	0.042	0.006
	3 December 2020	11	Assmannshausen	532.9	870	3.15	0.24	1.7 (80?)	6.6 (50?)	0.087	0.001
Lower Rheine	21 June 2021	9	Porz	681.3	2012	3.08	0.21	13.2 (63.4)	23.1 (18.6)	0.086	0.026
	22 June 2021	9	Rheindorf	703.6	1963	3.1	0.20	14.4 (44.9)	20.7 (13.8)	0.079	0.007
	23 June 2021	9	Urdenbach	720	2079	3.06	0.19	13.8 (57.6)	20.9 (18.8)	0.079	0.024
	24 June 2021	9	Uedesheim	729.3	2204	2.77	0.20	11.5 (37.9)	19.8 (13.1)	0.075	0.034
Lilar Lower Rheine	2 November 2021	8	Schenkenschanz	859	1052	3.42	0.14	17.9(36.3)	6.6 (8.5)	0.082	0.014
	4 November 2021 (only active width)	3	Schenkenschanz	859	1037	3.52	0.14	19.5(34.4)	6.7 (7.4)	0.082	0.027

Abbreviations: H, mean cross section depth; Q, mean discharge; D_{50} and D_{90}, characteristic bedload particles; Q_s, mean bedload transport rate of all positions and samples; $u*$, shear velocity; D_{50grab} and D_{90grab}, particles collected by a mechanical grabber with a depth between 20 and 60 cm, representing riverbed surface material; CS, cross section.

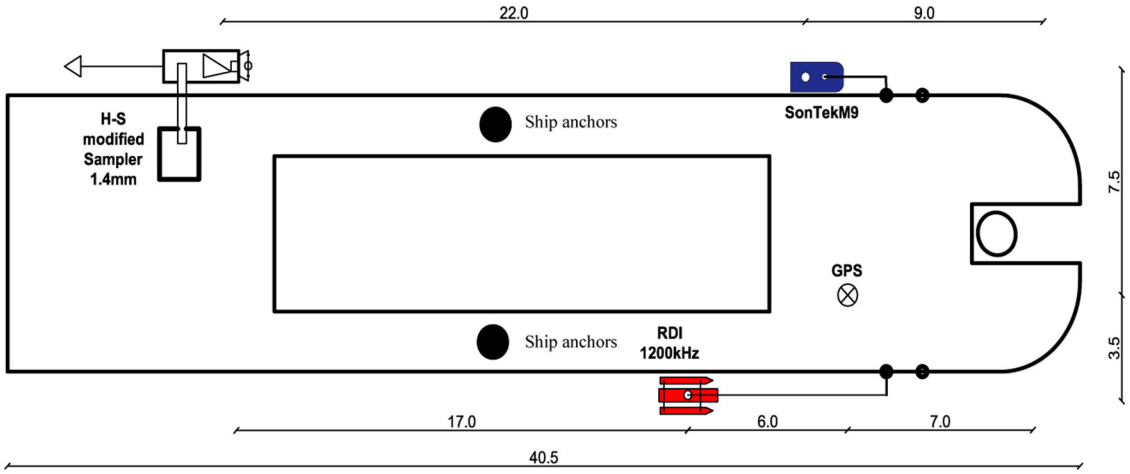

Figure 1 Experimental set-up, example of the instrument positions relative to the ship

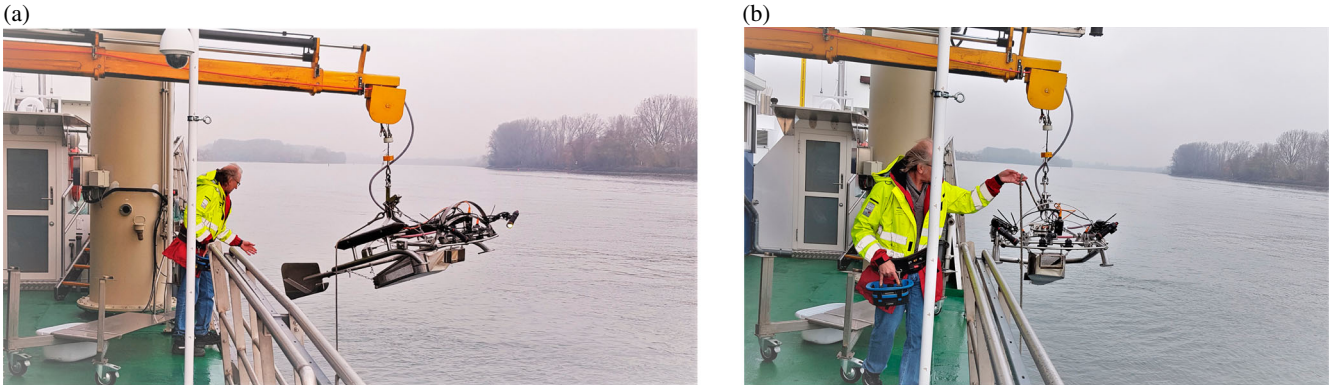

Figure 2 BfG bedload sampler in operation. (a) Side-look of the BfG bedload sampler in operation. (b) Front-look of the BfG bedload sampler in operation

(Vries, 1979). The BfG sampler is equipped with a steel basket with a 1.4 mm mesh size (note that the bottom does not have a mesh); a nozzle with 16 cm width and 10 cm height; the total length of the sampler is 91 cm, without the landing structure. To facilitate the landing and to ensure contact with the riverbed, the sampler is mounted on a steel frame and the nozzle neck is made of flexible plastic material (Fig. 2). As with all other direct bedload samplers, the BfG sampler suffers from different measurement inaccuracies, which generally result in only a portion of the material transported at the location of the measurement being collected by the sampler. Therefore, the results from the sampler require a calibration factor and the efficiency depends on the amount of sediment caught (Vries, 1979). The BfG sampler was developed for use in larger rivers like the Rhine with coarse sandy and gravelly bedload material. For a bedload material with a larger proportion of fine grain sizes, a lower efficiency must be expected, e.g. from losing material while lifting up or clogging the mesh (Brandstetter et al., 2012; Gaweesh & Van Rijn, 1994). The efficiency of the sampler was also tested with different transport conditions and PSD, resulting in calibration factors (Hubbell, 1964) that are used to correct the measured transport rate (Banhold et al., 2016). The calibration factors mostly depend on the total collected bedload mass and the hydraulic efficiency related to its design, and in this study varied between 1.1 and 1.5.

Based on the observations of the cameras mounted on the sampler some measurements were discarded due to unreliable sampling. At some positions, a large deviation between the three samples was an additional indicator to exclude these samples from further analysis (Conevski et al., 2020a). The final processing of the data is simple averaging of the valid samples per position.

2.4 *ADCP working principle, acoustic properties, and data pre-processing*

ADCPs are active ultrasound instruments, for which the working principle is sending an acoustic pulse with a pre-defined length (e.g. depending on the instrument's working frequency and configuration), then receiving the reflected signal with the same transducer (RDInstruments, 2011). The received signal is then analysed internally to obtain the well-known ADCP outputs such as the echo intensity, velocity and depth. The determination of the velocity is based on the "Doppler shift frequency" (RDInstruments, 2011). ADCPs are generally configured as an assembly of four transducers spaced at 90° azimuth intervals (i.e. Janus configuration). These transducers form acoustic beams with a grazing angle of 70°–60° that allows 3D velocity estimation, under the assumption that the velocity is homogeneous in the sampling plane of all four

beams. The sampling geometry of the four beam footprints was reviewed in Rennie et al. (2002), Rennie et al. (2017), and Conevski et al. (2020a). The ADCPs have two operating modes: water profiling (WP) mode and BT mode. The working principle is the same, but the BT mode uses longer pulses, which are supposed to contain more energy and allow the sound beam to ensonify the bottom over the entire beam width all at once (R. Conevski et al., 2020a; Lee Gordon & Instruments, 1996; Rennie et al., 2017). The BT is used for identification of the riverbed (i.e. water depth) and determining the velocity of the vessel, v_{BT}. For stationary deployment (Fig. 1), the BT signal is affected by the riverbed mobility, particularly, the BT velocity is equal to the apparent bedload velocity, $v_a = v_{BT}$. This velocity (v_a) is considered a measure of the spatially averaged bedload velocity (Rennie et al., 2002). Note that the determination of the BT velocity is more complex than the WP water velocity because the Doppler shift differs from one edge to the other of the acoustic footprint and it strongly depends on the rough riverbed surface and the acoustic properties of the instrument (R. Conevski et al., 2020a; Lee Gordon & Instruments, 1996). Due to this complex scattering process, the acoustics measurements are often affected by noisy data (Conevski et al., 2019), therefore filtering of the time series is necessary. The filtering procedure involves: (i) threshold de-spiking and vector filtering (i.e. eliminating all values exceeding three standard deviations from the mean or with opposite direction of the flow) as described in Conevski at al. (2019, 2020a); (ii) elimination of the data exposed to waves (e.g. sudden changes of the pitch-roll or spikes in the GPS); (iii) eliminating the velocities for which values were equal or larger than the velocity of the last WP cell (i.e. closest to the bed). The filtered time series were averaged to get the final apparent bedload velocity, v_a.

Besides the apparent bedload velocity, both ADCPs deliver the BT echo intensity in instrument units (EI). The determination of the EI internally in the ADCPs is not clearly explained by the manufacturer, but could be interpreted based on trailing, leading edge, or the centre of the echo distribution (Conevski et al., 2020a; Conevski et al., 2020b; Rennie et al., 2017). This signal contains information from both the mobile bedload particles (i.e. volume scattering S_v) and the immobile bedload particles beneath the active bedload layer (i.e. surface scattering S_s). Investigating the sensitivity of the BS strength towards the bedload characteristics requires derivation of a modified sonar equation (Conevski et al., 2020b):

$$B_S = 10\log(S_s + S_v) = -S_{L0} + k_{dB}(E_I - E_r) - A_f + 2\alpha R + 20\log(R) - P_{dB} \quad (1)$$

where S_{L0} is the source level calculated using the transmit voltage and currents present in the RDI output files or the pressure at the transducer, P, in the Sontek output file, as suggested by Shields (2010) and RDI (RDInstruments, 2015). k_{dB} is scaling factor to dB, E_r is the noise level, R is the slant distance to the sediment bed. The transmission losses in two directions include beam spreading $20\log(R)$ and the attenuation in the water column ($2\alpha R$) that accounts for the absorption due to water viscosity (Medwin & Clay, 1998) and the suspended sediment attenuation in the water column. The suspended sediment attenuation coefficient was calculated using the mean SSC and median diameter measured at the same time or for similar discharges. Nevertheless, the averaged SSC varied from $20\,\mathrm{mg\,l^{-1}}$ to maximum $170\,\mathrm{mg\,l^{-1}}$, resulting with a maximum of $0.1\,\mathrm{dB\,m^{-1}}$, although the median diameter was generally very fine (0.001–0.5 mm), corresponding to the prevailing viscous term (R. J. Urick, 1983). The attenuation in the active bedload layer is not taken into consideration and it is accounted as a bias in the BS strength. P_{dB} is the transmit voltage, and A_f is the area of the surface scattering at the bed, which is usually applied to normalize the surface backscatter for the unit area. More details about the parameters are given in the laboratory experiments presented in Conevski et al. (2020c).

2.5 *Temporal analysis and classification*

The nature of the bedload transport is characterized by a sporadic, inhomogeneous motion of particles, particularly in gravel riverbeds (Wilcock et al., 2009), which makes the transport spatially and temporally variable. Characterization of this variability is crucial for understanding the bedload processes, as well as their impact on the river morphology. Analysis of BS strength and the apparent bedload velocity using signal processing tools have demonstrated that there are short-term variations that are usually lost after averaging the time series (Conevski et al., 2022). In this study, the wavelet transforms analysis of the signal is performed to understand better these short-term nonstationary effects (Foufoula-Georgiou & Kumar, 1994). The wavelet analysis permits studying local features of non-stationary signals, in frequency and time, where the Fourier transformations usually fail (Foufoula-Georgiou & Kumar, 1994). The analysis is presented through the wavelet spectrum (i.e. scalograms), which represent an absolute value of the continuous wave transformation (cwt) coefficients plotted as a function of time and frequency. The cwt enables time-frequency analysis of the time-series of both variables, aiming to identify the local (e.g. bursting of patch of sediments, ripples superimposed on the dune, etc.) and global (e.g. dune mobility) periodicities of the bedload transport. The 2-D visualization of the cwt on the ADCP variables helped for identification of the instantaneous bedload characteristics, such as bedload rate intensity and granulometry variation. Moreover, the cwt could also identify some periodic noise sources that can be related to the ship, the instrument or the natural environment at the study site.

Finally, the post-processed ADCP BT outputs (v_a, B_s) and some statistical variables obtained from the same time series were clustered using unsupervised machine learning (ML) approach (i.e. Gaussian mixture models, GMM). The main motivation is to demonstrate that a rather simple application of

the ML method on the ADCP outputs could be a stand-alone tool to classify the bedload transport conditions. The GMM used in this study are based on K-independent Gaussian distributions that are used to model the separate clusters (Jothilakshmi & Gudivada, 2016). The GMMs are considered more robust and more suitable for data with several inputs (Jothilakshmi & Gudivada, 2016). The GMM returns the cluster centroid and cluster variances for a family of points if the number of clusters is predefined (i.e. training phase). The centroid and variance can then be passed to a Gaussian probability distribution function to compute the similarity of an input query point with reference to a given cluster (i.e. evaluation phase).

3 Results

The results section is divided into three parts: (i) the mean values analysis of the ADCP outputs versus bedload intensity and the bedload PSD which elucidates the reciprocal sensitivity; (ii) time-frequency analysis of one randomly chosen measurement; (iii) bedload classification applying GMM to ADCP outputs.

3.1 *Backscattering strength sensitivity towards the bedload intensity and bedload grain sizes*

The temporal mean values of the BS strength (B_s) are plotted against the bedload intensity, which in this case is represented by the apparent bedload velocity (v_a). The B_s is the average of all four slant beams (e.g. for 1.2 MHz, RDI and 3 MHz, M9) and v_a is calculated using the homogeneous assumption of the beams. Both variables are filtered and de-spiked as explained in section 2.4. It is assumed that v_a represents the bedload intensity, better than the physically measured transport rate, due to a few reasons: (i) the spatial consistency of the v_a and B_s, knowing that the sampler is some 15–20 m away from the ADCPs sampling area (Fig. 1); (ii) temporal alignment between ADCP derived data, avoiding any deviation among the periods of operating the physical sampler; (iii) the possible inaccuracies introduced by the BfG-sampler, especially in weak transport conditions and uneven riverbed (Conevski et al., 2020a; Gaweesh & Van Rijn, 1994). By deploying v_a as an indicator of the bedload intensity, the invalid samples, measured by the BfG sampler (i.e. which are discarded in the other analysis) are actually included in this comparison and marked with the x-symbols in Fig. 3.

Figure 3a–c show that the B_s values for 3, 1.2 and 0.5 MHz (vertical beam, M9) are decreasing as the intensity of the transport increases. This was most obvious for the 3 MHz, most likely due to the highest working frequency and smaller grazing angle (65°), which implies the highest losses in the active bedload layer and prevailing volume scattering (Conevski et al., 2020b). It could be also noticed that there are two trends, which represent sand-dominated (red arrow, Fig. 3a) and gravel-dominated riverbed (blue arrow, Fig. 3a). Note that there is not a precise distinction between sand and gravel, knowing that in most of the gravel-dominating measurements, there is also a high partition of sand. The highest bedload intensity, the sandy data from Oder (Table 1), seems to lay between these two trends (small triangular symbols Fig. 3a), most likely due to the increased ambient noise (which is not modelled) and presence of debris in the bedload transport. Some outliers are also visible in Fig. 3a, which are identified as ADCP-biased measurements. These data contain erroneous measurements of the apparent bedload velocity: the shaded rectangles in the lower part of Fig. 3a represent, for example, the flow of leaves, debris and shells that mimics the bedload transport velocity; the shaded rectangles in the upper part of Fig. 3a represent very rough bedload surface, rocks and stones, with no bedload transport. This confuses the Doppler shift estimation, resulting in false velocities (Medwin, 2005).

The 0.5 MHz vertical beam data looks more consistent, resulting in a smaller slope of the decreasing trend (Fig. 3b). This is explained by the vertical grazing angle and lower working frequency. The division into two groups of datasets (e.g. gravel vs sand) is also visible here, but there is no obvious change in the trends. Note that *va* has the same data as for the 3 MHz (i.e. only the slant beams can be used for velocity estimation).

The 1.2 MHz, RDI, similarly to the laboratory experiments (Conevski et al., 2020b), showed low sensitivity towards different bedload transport conditions (Fig. 3c); penetrating the active bedload layer and dominantly scattering from the immobile surface below. Two trends may again be identified: one, which is more inclined, the data that is more scattered both due to the rough surface of the coarse armoured layer or bedforms (black arrow, Fig. 3c), and another that is almost vertical, that includes the data with moderate to abundant transport rate (right, Fig. 3c). The outliers are not easy to identify, because the data do not distribute with evident correlation. Nevertheless, the sandy data on the right of Fig. 3c represent sand passing on top of an armoured/rocky layer in Middle Rhine 498.3 km (Table 1), and could be identified as outliers deviating from the general trend. In the middle Rhine, there is predominantly gravel but in average or below average flow there are patches of relatively intensive sand-gravel transport, as was the case in some of the campaigns (Table 1). Note that RDI uses BB-coded signal processing which enables higher resolution profiling and acoustic sampling through the entire active layer (Conevski et al., 2020a, 2020b).

For the M9 – 3 MHz, it was observed (Fig. 4a) that the coefficient of variation of the BS strength (Cv_{BS}) slightly increases as the coefficient of variation of the bedload apparent bedload velocity (Cv_{va}) increases. It is also noticeable that the variation of the v_a is higher for the gravel data or the data with no reliable physical bedload measurements. This follows the laboratory tests (Conevski et al. 2020b), suggesting that the higher bedload transport intensities trigger more deviation in the results. The M9 – 0.5 MHz resulted in a rather stable variation of

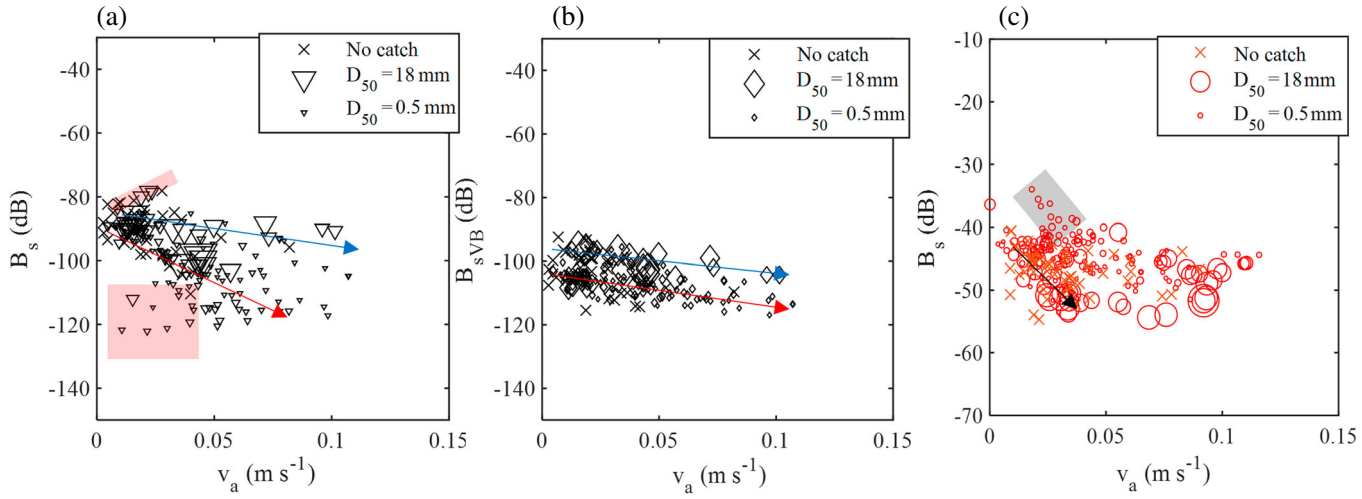

Figure 3 Apparent bedload velocity (v_a) as an indicator of the bedload transport intensity against the BS strength (B_s). (a) Data extracted from M9 3 MH – IC; (b) data extracted from M9, vertical beam (VB) 0.5 MH – IC; (c) data extracted from RDI 1.2 MH – BB; the × symbols indicate that the bedload measurement was unreliable, or there were no data at all, thus these points were not used in the calculations

the backscattering strength and was very low (Fig. 4b, ~0.05). This further corroborates the finding that volume random scattering from moving particles (i.e. the active layer) prevails in a condition of greater mobility while fixed reflection from immobile particles (i.e. surface scattering) overlaps in low transport conditions. Similar to M9 – 0.5 MHz, 1.2 MHz gave low *Cv* values, also due to the influence of the surface scattering, but as a consequence of the finer resolution and BB signal processing (Conevski et al. 2020a).

In Fig. 5 the correlation between B_s and the median diameter (D_{50}), calculated from sediment caught by the BfG sampler (i.e. only mobile particles), is presented for the three frequencies used in this study. The 3 MHz shows no correlation with D_{50}, and this complies with the previous comment that the volume scattering of moving particles prevails. Moreover, the 3 MHz IC also performs more superficial sampling of the active layer due to the lower resolution of the bin profiling (Conevski et al., 2020b), resulting in less sensitive data toward the shape of the particles (D_{50}). The prevailing volume scattering is visualized with the negative trend (Fig. 4a, red line) that demonstrates the loss of the BS strength within the active layer for the sandy environment (also in Fig. 3a). The B_s for the gravel data (group of points on the right in Fig. 5a) seem to stay stable for all points, most likely due to the shallow and insufficient ensonification of the riverbed (i.e. shorter pulse length and coarse profiling) and smaller grazing angle for the M9 (65° for M9, 70° for RDI).

On the other hand, a positive correlation between B_s and D_{50} was observed for the 0.5 MHz (Fig. 5b), which complies with the fact that the impact of the volume scattering is minimal, and that surface scattering prevails at a 90° grazing angle and lower working frequency (Conevski et al., 2020b). For example, in most of the cases, the difference between sand and gravel is about 5 dB. The vertical beam also shows a direct reflection of the riverbed and minimizes the refraction losses, making the D_{50}–B_s relation stronger (Urick, 1983), knowing that the static bed and bedload have similar PSD (Table 1). For negligible sound attenuation, the increase of the BS strength with an increase in the grain size complies with the Rayleigh scattering theory, which states that larger particles have stronger backscattering properties (Medwin, 2005; Moate & Thorne, 2009). Therefore, the observed D_{50}–B_s positive correlation reflects an overall PSD coarsening which entails stronger backscattering for coarser fractions falling within the Rayleigh regime or a wider class reaching the geometrical regime (i.e. maximal scattering strength for given frequency).

The RDI 1.2 MHz data behave differently than the M9 and forms an asymmetrical parabolic function (Fig. 5c) that implies the signal penetrates the active layer. For sand-dominated environments, the sound propagation reaches the immobile particles; thus B_s starts to increase as the D_{50} enlarges, and that is the prevailing effect of surface scattering for sandy more intensive transport. In the upper part of the parabola, the BS starts to decrease at the transition from sand to gravel. This is a signal attenuation that might be ascribed to sound absorption-scattering within the active layer and reflection losses at layer interfaces (e.g. between the active layer and the armoured layer beneath). Particularly relevant for reflection losses, the rough surface of the immobile armoured layer coupled with the 70° grazing angle may broaden the reflected return in all directions within the active layer, therefore contributing to more diffusive loss (Conevski et al., 2020b; Ivakin, 1981). Furthermore, the RDI-BB coded signal processing enables much finer resolution, which coupled with the lower working frequency and enhanced the signal penetration within the active bedload layer (Conevski et al., 2020b; RDI, 2015). Concluding on that, reflection losses apparently prevailed for gravel beds. In this case, the immobile particles, which are typically larger than the sampled particles (Table 1), formed an acoustically rough and dispersive bed, with a roughness wavelength that

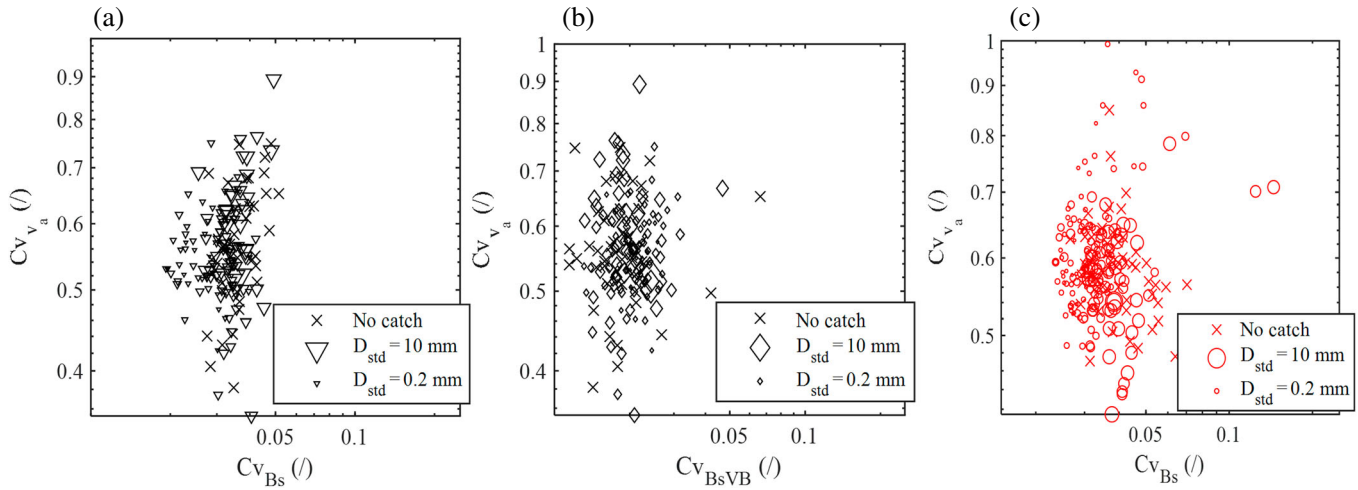

Figure 4 Coefficient of variation of the apparent bedload velocity (Cv_{v_a}) versus coefficient of variation of the BS strength (B_s). (a) Data extracted from M9 3 MH – IC; (b) data extracted from M9, vertical beam (VB) 0.5 MH – IC; (c) data extracted from RDI 1.2 MH – BB; the size of the symbols indicates the standard deviation of corresponding PSD of the bedload caught by the BfG physical sampler; the × symbols indicate that the bedload measurement was unreliable, or there were no data at all, thus these points were not used in the calculations

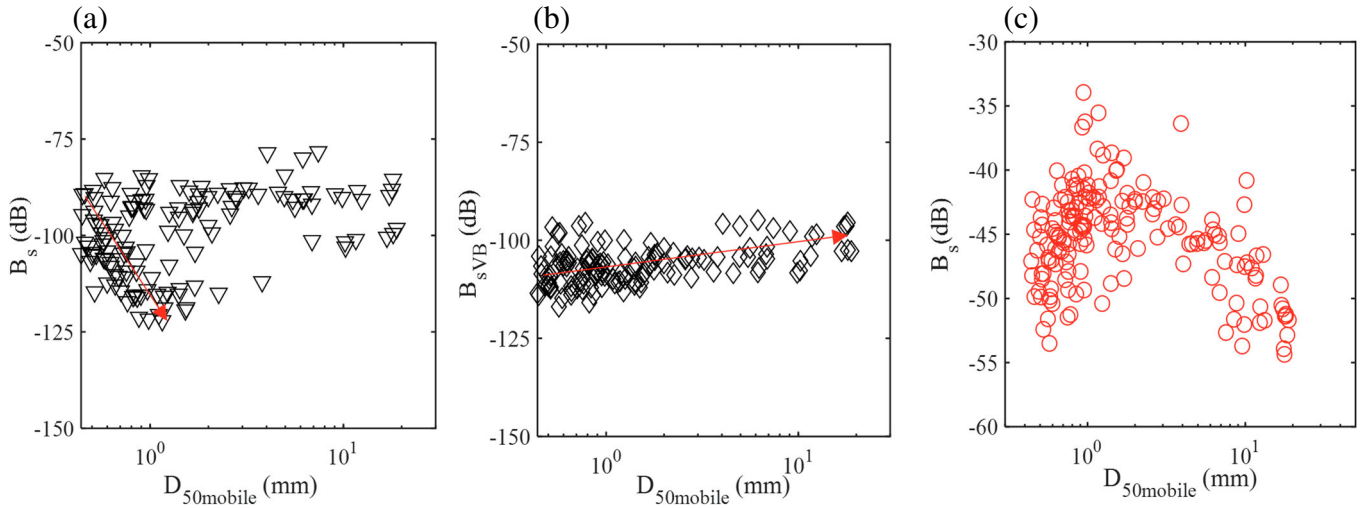

Figure 5 The median grain size (D_{50}) of the bedload (i.e. mobile particles) against the BS strength (B_s). (a) Data extracted from M9 3 MH – IC; (b) data extracted from M9, vertical beam (VB) 0.5 MH – IC; (c) data extracted from RDI 1.2 MH – BB

was significantly larger than the 1.2 MHz wavelengths (Urick, 1983).

The standard deviation (std) of the mobile particles is generally high, particularly in the case of gravel-bed rivers. However, the std of the M9 data is not correlated with the particle size deviation (not shown). This corroborates the finding that the 3 MHz performs superficial sampling, and the 0.5 MHz vertical beam results in prevailing surface reflection poorly affected by particles sorting within the active layer. On the other hand, the coefficient of variation for the 1.2 MHz B_s increases with the Cv of the grains, which agrees with the more efficient penetration and scattering of sound throughout the active layer.

Note that in Fig. 5, ∼10% fewer samples were analysed, because only the samples with bedload transport rate larger than 0, ($Q_s > 0\,\mathrm{kg\,m^{-1}s^{-1}}$), were considered, where PSD is available and the samples for which poor sampling was observed, with the camera, were eliminated.

3.2 *Time-frequency analysis of v_a and B_s*

One measurement/position of cross-section 703.6, in the Lower Rhine River (Table 1) was chosen to visualize the temporal and spatial variability of the bedload data by using cwt and scalograms (i.e., plotted cwt in time and frequency). The information from the scalograms will help understanding the bedload characteristics at different instances. The measurement was chosen randomly among the ones that contain valid information from the BfG-bedload sampler. The physically measured sample had the following characteristics: median grain size equal to $D_{50} = 7$ mm with 35% content of sand; mean transport rate equal to 35 g s^{-1} m^{-1}, which makes for weak to medium bedload transport conditions, dominated by gravel particles.

The calculations were performed in Matlab using the cwt function where the analytic Morse wavelet was used as a mother wavelet for decomposition of the signal, with symmetry

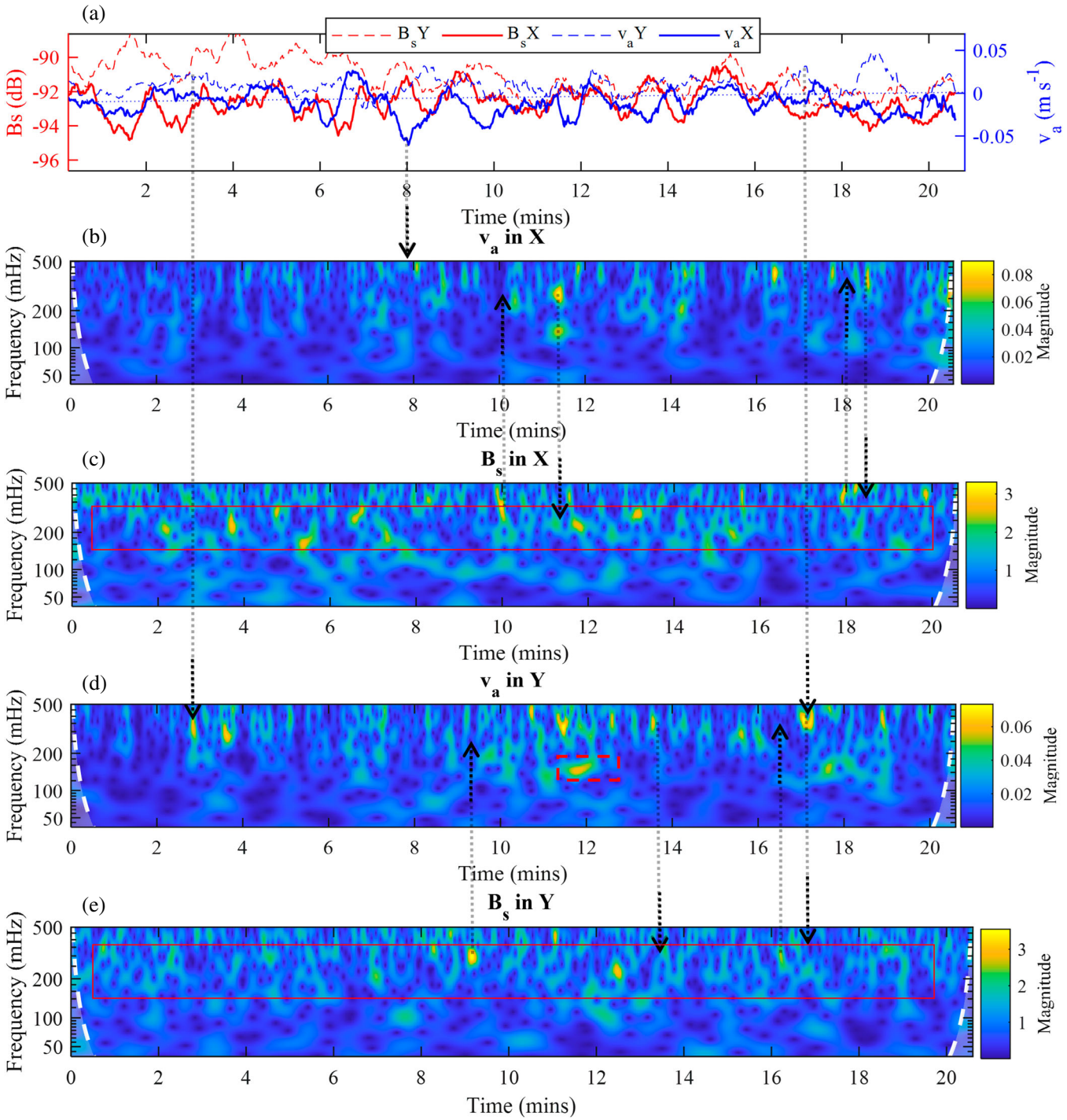

Figure 6 Time frequency analysis of the $v_a - B_s$ in both X (beam 2–4) – Y (beam 1–3) ADCP oriented directions. (a) moving mean (window, [15 15]) of v_a and B_s in Y direction (dotted line) and in X direction (full line); (b) cwt of v_a in X direction; (c) cwt of B_s in X direction; (d) cwt of v_a in Y direction; (e) cwt of B_s in Y direction

parameter, gamma, equal to 3 and the time-bandwidth product equal to 60 (Lilly, 2017), which means perfectly symmetric. The maximum frequency limit presented in the scalograms is determined based on the Nyquist frequency, whereas the maximum period limit cannot exceed the signal length divided by the product of two times standard deviations of the wavelet and the wavelet peak frequency (Lilly, 2017). The total length of the registered data by the ADCP was 20.4 min, with sampling rate of 1s, therefore allowing a comprehensive investigation of the variation in time.

The cwt analysis of the data shown in Fig. 6 is from the M9 working at 3 MHz – IC and it is divided into X–Y instrument directions (i.e. averaging the data of beam 2–4 and beam 1–3). By doing this the spatial variation of the bedload, at a local scale, is considered. The ADCP was positioned in a way that the Y-direction is the main flow direction.

Figure 6 shows higher magnitudes of the cwt coefficients and a tendency of motion in the Y-direction, at the same time in the X-direction, until 7 min there is almost no motion (blue lines, Fig. 6a), although v_{ax} is changing sign, crossing the zero, 7 times until min 7. At the beginning of 7 min, there is a pulsation of v_{ax} in a positive direction and then negative at min 8; after that the motion in the X-direction is dominantly in a negative direction. This is also visualized in the $v_a$magnitudes of the cwt coefficients (Fig. 6b, c), which have the same time resolution as the data. For the both X–Y directions, until the 3 min, there is no transport, except possible weak fluxes of some sand-organic mixtures (Fig. 6a–e), then movement is visible in the Y-direction and increase of the v_a, followed by a decline of the B_s (Fig. 6d, e). Near the end of the time series, v_a increases in both directions and the transport occurs at higher frequencies (e.g. 500 mHz). At the same time, the BS strength in the X-direction is stronger with oscillations that appear between 150–300 mHz present almost the entire measurement (long red rectangle, Fig. 6c), most likely due to sampling directly on rocks stones falling within the acoustic footprint of beams 2–4, as well as due to the uneven riverbed (Fig. 7). In the Y-direction an aggregation of energy was observed, but fewer peaks in this interval (150–300 mHz), which is due to beams grazing towards the flow direction (red rectangle, Fig. 6e). In Y-direction the B_s is lower and more attenuated due to the more intensive transport, resulting in lower cwt magnitudes at the frequencies where the v_a intensifies (e.g. between min 3 and 4 as well as at 12 and 18 min). Interestingly, before and/or after each peak of v_a cwt magnitude, there is also an abrupt change of B_s magnitude (see the arrows in Fig. 6). This phenomenon is also illustrated in Fig. 8, where two sequences are cut from the time series for v_a and B_s and plotted one against another. In the period between minute 9.5 and minute 10.5 (Fig. 8a) there is a tendency to decrease the velocity in X-direction and increase the BS strength by 2 dB, which implies intensifying of the surface scattering. At the same time, in the Y direction, the values of v_a and B_s remain invariant, with a slight tendency to increase (see also Fig. 6d, e). On the other hand, Fig. 8b (at 18–19 min) demonstrates negative correlations between v_a and B_s, reflecting the increase in the apparent velocities, the bedload transport intensity, and the thickness of the active layer. The intensity is higher in the Y-direction.

Moreover, looking at the high-frequency events, it appears that some information is missing and that the 1 Hz sampling of the ADCP is unable to fully describe the non-stationary fluctuations of the bedload transport (upper right part of Fig. 6b–d).

The final comment is related to the lower frequency peak at 150 mHz and 12 min in both Fig. 6b and d (dashed red rectangles), which shows fluctuations of the velocities, most likely due to the passage of the ship (registered in the field notes). Registering low cwt magnitudes in the BS strength at these frequencies shows the possibility of eventual water bias (Rennie et al., 2002) most likely initiated by the hydrodynamic pressure of the nearby ship passage.

Table 2 Parameters in the GMM unsupervised ML model. Please note that the results of each combination of inputs are shown in Fig. 9.

ADCP	Inputs	Clusters
M9 3 MHz, 0.5MHz, (Fig. 9a)	v_a, B_s, [a] std(v_a), std(B_s), [b] FD, [c] v_a^{err}, $B_{s\,\mathrm{VB}}$, std(B_{sVB})	5
RDI 1.2 MHz, (Fig. 9b)	v_a, B_s, std(v_a), std(B_s), FD, v_a^{err}	5
M9 3 MHz, (Fig. 9c)	v_a, std(v_a), FD, v_a^{err},	4
RDI 1.2 MHz, (Fig. 9d)	v_a, std(v_a), FD, v_a^{err}	3

[a]std refers to the standard deviation of the variable
[b]FD percentage of filtered data (Conevski et al., 2019)
[c]Bottom track, error velocity (RDI, 2015)

3.3 *Bedload classification using ADCP outputs as input: v_a and B_s*

The correlations given in Figs 3 and 4 supported the possibility of developing a statistical or machine learning model that could classify the data. To evaluate the ADCP outputs in the least biased way, an unsupervised machine learning (ML) model, GMM, was used to classify the data, using the mean and std values of the filtered B_s and v_a as inputs (Table 2). In two scenarios, four tests were performed, with and without the BS strength in the input variables for the M9 and the RDI (Table 2). The main purpose was to demonstrate that the BS has an added value to a better representation of the bedload transport. The unsupervised ML models do not require targets to calibrate (i.e. Q_s and/or D_{50}) but use only the features derived from ADCP outputs. The GMM were applied both to the 3 MHz M9 and 1.2 MHz RDI datasets, after performing normalization of the inputs. The number of clusters and the parameters of the GMM models were optimized in a trial-and-error procedure using Akaike's information criterion for the estimated model (Jothilakshmi & Gudivada, 2016).

Figure 9 presents four plots of D_{50} vs $Q{*_s}$, where $Q{*_s}$is a dimensionless transport rate (Van Rijn, 1984), in which the assigned colours are the clusters estimated by the GMM, using only the ADCP data (Table 2). Remarkably comparable results were obtained for both datasets, the M9 and the RDI (Fig. 9a, b), identifying five optimal clusters that were classified based on the transport conditions, no transport, weak to moderate transport conditions; and according to the granulometry gravel to sand data (Table 3). In general, there are three clusters (e.g. cyan, green and blue in Fig. 9a, b) that are associated with sand transport and one that is associated with gravelly dominated transport

Figure 7 Picture of the riverbed nearby the example presented in Fig. 6 (wavelet analysis)

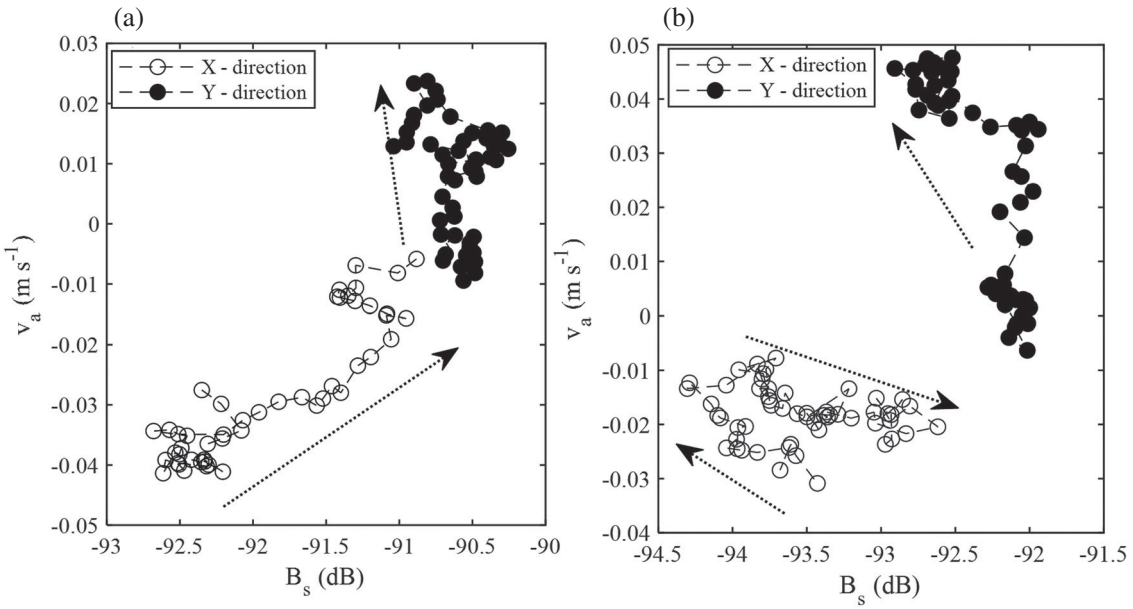

Figure 8 $B_s - v_a$ raw data, time instances from the identified form the cwt analysis in both directions X–Y (Fig. 5). (a) $B_s - v_a$, between 9.5 min and 10.2 min, also shown with arrows in the cwt magnitudes. (b) $B_s - v_a$ between 18 min and 19 min, also shown with arrows in the cwt magnitudes

(black). This corroborates with the conclusions given in Rennie et al. (2017), that ADCP data collected in a gravel river significantly differ from those in sandy rivers. The GMM seemed to perform better for the M9, establishing a cleaner distinction between gravel and sand with less overlapping and little double membership in the clusters, most likely because of the vertical beam data (i.e. 0.5 MHz), which strengthened the input information regarding the D_{50} in the GMM. The green cluster in both Fig. 9a and b is overlapping with the other clusters because it is the transition from weak to moderate transport conditions, which involves the formation of bedforms. In both datasets, 20% of the points share more than one cluster. The zero-transport values are represented in the separated fifth cluster which is not visible in Fig. 9. However, it can be noticed that some other clusters also partition in the fifth cluster as outliers due to existing outliers in the datasets, discussed in the next section.

Figure 9c and d show results from GMM without the BS strength variables (Table 2); the classification seems to be less efficient in defining the clusters. This is particularly visible for

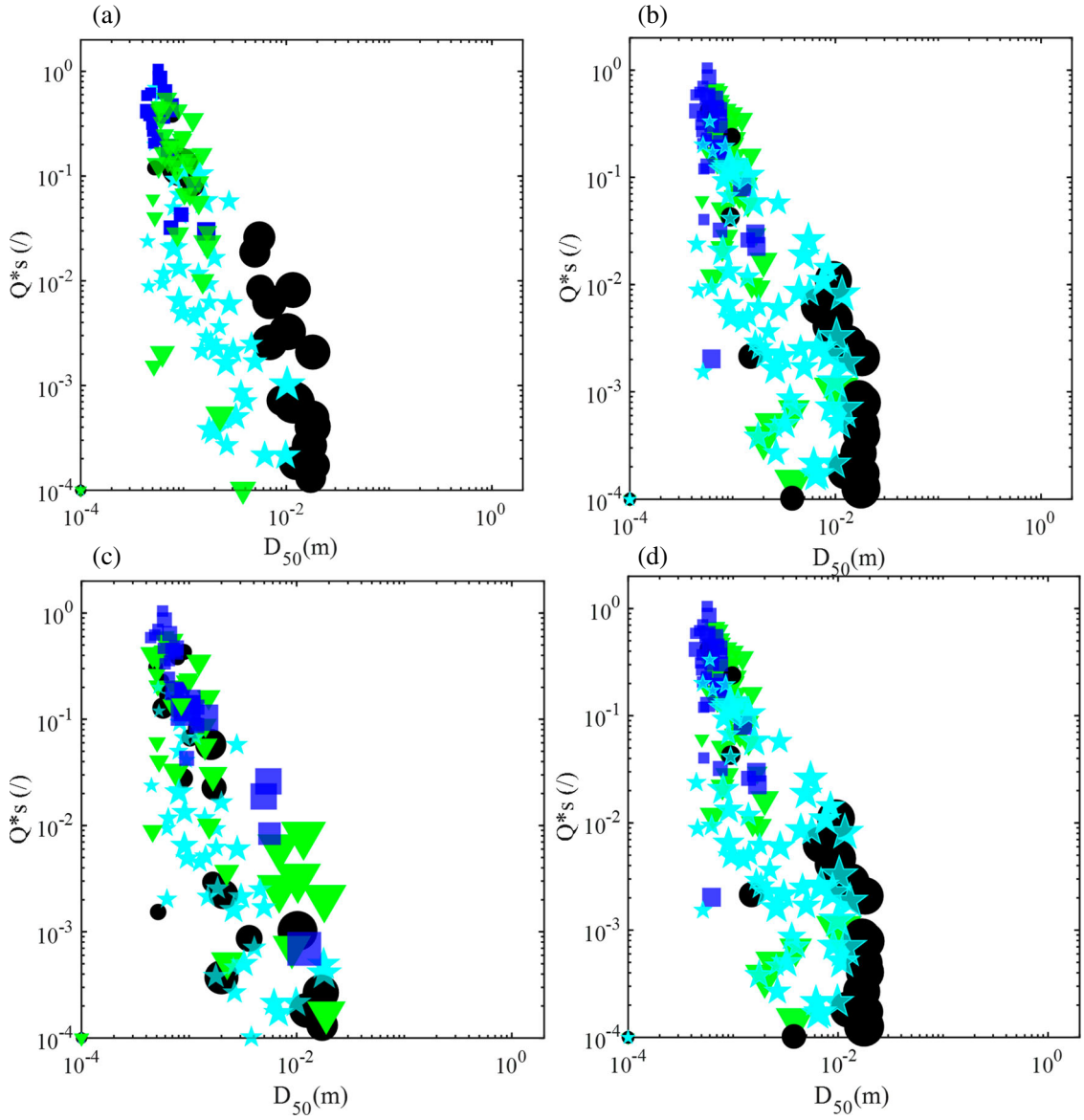

Figure 9 Plots of D_{50} vs $Q{*}_s$ where $Q{*}_s$ is dimensionless transport rate measured by the sampler, and D_{50} the median sediment particle size. The clusters (Table 3, a qualitative explanation of the clusters of each plot) are showing the results from the GMM applied using only the ADCP outputs (Table 2). Note that D_{50} vs $Q{*}_s$ is used only to visualize the clusters and these variables are not use in the clustering. (a) M9 3–0.5 MHz, including both v_a and B_s; (b) 1.2 MHz RDI, including both v_a and B_s; (c) M9 3–0.5 MHz, including only v_a (d) 1.2 MHz RDI, including v_a. In all plots the size of the symbols is proportional with the std of the mobile bedload PSD at that position

the M9 (Fig. 9c), where the GMM failed to distinguish among the different grain sizes. This is expected because the 3 MHz should be representing the velocity at the top of the active layer and in this test the vertical beam data are not used. The GMM using v_a from the 1.2 MHz delivered somewhat better results, giving the optimal solution for only three clusters (Fig. 9d), producing two weak transport clusters, gravel (back circles, Fig. 9d) and sand (cyan stars, Fig. 9d) and good to intensive sand transport conditions (blue squares, Fig. 9d). The GMM were unable to cluster the no-transport values in the last test, having only the v_a-related inputs (Table 2).

Further parameter optimization of the GMM could possibly result in better clustering, but it is out of this study's scope. The obtained results demonstrate that the ADCPs alone give enough information reflecting the most important bedload parameters variation (i.e. $Q{*}_s$ and D_{50}).

4 Discussion

4.1 *Sources of uncertainty in the ADCP outputs and backscatter sensitivity*

Figures 3 and 5 showed that the BS strength is sensitive to the bedload intensity and the PSD of the bedload (Conevski et al., 2020b). It was also presented that the field measurements are more complicated, entailing many external factors that might disturb the measurements and eventually introduce more noise and outliers. Some of those can be easily eliminated

Table 3 Qualitative description of the clusters and outliers in Fig 9, based on inputs in Table 1.

Cluster	Fig 9a M9 3/0.5MHz	Fig 9b RDI 1.2 MHz, w/o B_s	Fig 9c M9 3/0.5MHz,	Fig 9d RDI 1.2 MHz, w/o B_s
1 No symbol	No or very weak bedload transport.	No or very weak bedload transport.	No or very weak bedload transport.	N/A
2 Black	Gravel transport weak to medium. With 4 outliers in the sandy area, with high std of the PSD.	Gravel transport weak to medium, with 6 outliers.	Weak transport, both sand and gravel. With 4 outliers in the good transport conditions.	Weak transport, both sand and gravel. With approx. 10 outliers in the good transport conditions.
3 Cyan	Sand or mixtures weak to good transport conditions.	Sand or mixtures weak to good transport conditions. Overlapping with the gravel dominated.	Sand or mixtures of sand and gravel; weak to good transport conditions.	Sand or mixtures weak to good transport conditions. Outliers in the weak gravel transport conditions.
4 Green	Sand transport good to abundant, the transition class.	Sand transport good to abundant, overlapping with class 2.	Gravel and sand mixtures, overlapping without clear division	N/A
5 Blue	Sand intensive transport and/or good to abundant	Sand intensive transport and/or good to abundant. 6 outliers that are in the weak transport area.	Sand intensive transport and/or good to abundant. With 4 outliers that are in the weak transport area.	Sand intensive transport and/or good to abundant, with some outliers that are in the weak transport area.

but a certain on-site knowledge must be used. During these extensive campaigns, the following sources of uncertainty were observed:

- Passage of leaves and wood near the riverbed during the autumn measurements, resulting in false v_a and attenuated B_s.
- Passage of large cargo ships near the measuring set-up, influencing the apparent bedload velocity estimation. The appearing surface waves affect the water velocity and the apparent bedload velocity filtering (Conevski et al., 2019), as well as potentially producing a water bias (Rennie et al., 2002), affecting only the apparent bedload velocity.
- Patches of shells and algae moving at the riverbed during high-water velocities, causing false v_a, similar to the leaves.
- Highly uneven riverbed, rocky bottom, or large submerged gravel bars, resulting in inhomogeneity of the beam data, different BS values and false v_a.
- Mats of algae carpeting the rocks at the river bottom (particularly close to banks in low-velocity areas), contributing to lower, false BS strength. In addition, if these algae are swirling with the flow and/or if other underwater vegetation is present, it can result in false v_a values.
- An armoured layer, or a layer of rocks and intensive fine gravel-sand transport on top of it. In these cases, the BS strength values were higher and not representative of the sand and fine gravel. In particular, the lower frequency measurements were biased towards the layer of immobile stones below and not to the mobile bedload.

Another important source is the natural variability of the bedload, which is emphasized in the weak transport conditions and gravel riverbeds. Some of the BS data could be underestimated in these cases due to the final averaging of the results. Moreover, the comparison with traditional methods (i.e. pressure difference samplers) should not be taken for granted. On several occasions, the sampler was not able to properly catch the bedload transport due to: (i) landing on the lee side of the dune, resulting in sand pausing below the sampler, causing a scouring effect; (ii) landing on rocky bed with intensive sand-gravel transport on top of it. In these cases, the B_s interpretation would be wrong, as well as the v_a to Q_s comparison.

4.2 *Practical information from the temporal and spatial variations*

The temporal analysis using cwt in the two main instrument directions allowed better interpretation of the bedload transport

in time and frequency. It provided information for the temporal variability and, by using the data from separate beams, also for the spatial uniformity. The peak energy accumulations in a certain period, resulting in high v_a values, showed that the averaging of the long-term time series could lead to a wrong interpretation of the bedload transport, especially if it is gravel dominated. This gives particular importance to the vector filtering procedure (i.e. eliminating all velocities in the opposite direction of the main flow), but also a consistent mismatch with the bedload sampling data. Moreover, the abrupt accumulation of energy with high v_a yet low B_s (Fig. 6b–e, black arrows) proved the negative correlation of the B_s versus v_a presented also in Section 3.1 (Fig. 3a), with these instances of decline of the BS strength presumably due to attenuation in the active layer during conditions of more intensive transport.

The low cwt magnitude in the X-direction (Fig. 6b, c) suggested that the four beams averaging of the ADCPs could be another source of uncertainty, e.g. a spatial inconsistency when calculating the mean B_s and the modulus of the velocity vectors measured by the ADCP, which is then compared to the sampler's data. In that case (Fig. 6), more reasonable could be a direct comparison of the v_a in the Y-direction, as the sampler was sampling the same direction in a considerably smaller area.

The lower frequencies' peaks in the cwt magnitudes (e.g. less than 200 mHz) could be also associated with turbulent events near the bed and bedforms (e.g. low-streak ejections, bursts) and the eventual presence of macro-turbulent structures (Nezu & Nakagawa, 1993). The bursting phenomena could appear in periods of 4–7s (i.e. 150–250 mHz) for shear velocities $u* = 0.04$–$0.1\ \mathrm{m\ s^{-1}}$ (Table 1), and initiate bedload as reflected in the apparent bedload velocity (Nezu & Nakagawa, 1993). However, a more detailed analysis must be performed to analyse the entire water profile of the ADCP measurements and correlate the water velocity close to the bed and the apparent bedload velocity. Moreover, the wavelets could help in identifying the pulsations (i.e. possibly initiated by macro-turbulent structures) of the bedload and thereby identify the periodical motions of gravel patches in mixed gravel-sand river environments (Fig. 6), especially if long time series of measurements are performed. For example, for Lower and Middle Rhine, it was noticed that the cwt magnitudes of the apparent bedload velocities, with a range of 0.04–$0.06\ \mathrm{m\ s^{-1}}$, could be associated with the pulsation of sand-gravel. Conversely, cwt magnitudes of the BS strength in the range of 2–3 dB can be associated with rough riverbeds (e.g. bedforms, rocks, coarse armoured gravel). This could be accompanied by more complex feature extraction using wavelet packet entropy, wavelet scattering, etc.

4.3 *Wavelet analysis for filtering*

The wavelets could also be used to improve the de-noising and filtering of the raw data. For instance, discarding the low frequency v_a data with high cwt magnitudes could contribute to more consistent v_a values, in this case, eliminating the false data affected by the nearby passing ships (Fig. 6, dashed rectangles). After an extensive cwt analysis of several different bedload conditions, the filtering procedure could be upgraded by introducing a low- or high-frequency pass filter, which would discard the erroneous velocities produced by the external disturbances.

4.4 *Classification of the ADCP data for different bedload transport conditions*

The effectiveness of the BS strength data in the improvement of a simple implementation of unsupervised models (e.g. GMM) proved the added value of the BS strength data in the qualitative and quantitative evaluation of the bedload transport. The importance of the BS strength was also presented in the other sections, but the GMM offered fast, simple, and coupled implementation of the ADCP variables, partially eliminating the ambiguity in the BS strength data (e.g. 1.2 MHz, Fig. 4). The most distinctive clusters were obtained by using the M9 data involving all beams, including the vertical one, which highlighted the fact that change of the angle helped the bed material recognition not being biased by a possible transmission in active bedload layer. A vertical beam and the possibility to change grazing angle would increase the received information about the bed material both for immobile and mobile particles.

It should be noted the unsupervised ML models might not be the best model choice, but the testing of more comprehensive models (e.g. supervised ML) is out of the scope of this study.

4.5 *Recommendations about analysis of the BS data in the field*

The joint analysis of the backscattering strength from the river bottom and the apparent bedload velocity supports a wider understanding of the bedload transport, but possible biases must be carefully evaluated. For example, the BS strength signal could be attenuated by the sand motion or highly scattered by the rocky armoured bed, thus a pre-knowledge of the sampling conditions is necessary to validate the BS data.

Regarding the bedload sampling: integrating cameras to the sampler as in this study is an advantage. In fact, many false samples were discarded based on videos. Also, in some cases (as explained above) the filtered v_a represents a more reliable choice for further analysis and comparisons. In the same manner, the weak transport conditions should be analysed with special attention. It is recommended to perform a visual check of the videos, if they exist, as well as spatial-temporal analysis as suggested in Section 4.2. This would allow more efficient filtering of the biased data. Finally, longer sampling times are recommended, especially in gravel environments characterized by pulsating mobilization events or in case of a disturbed environment (e.g. in the navigation channel during the passage of ships).

4.6 *Future research*

The next step of this research will be focused on detailed investigation of the structural and natural uncertainty for all types of the ADCP, bedload transport conditions and the grain size of the mobile particles, and finally advancing towards estimation of the total bedload transported masses.

Another example for future research efforts on this subject could be the implementation of the clustering method on moving boat ADCP measurements using RTK-GPS (Rennie & Church, 2010). The clustering method using the suggested variables (Table 2) on the entire data cloud would result in re-mapping the clusters of different bedload transport conditions. Furthermore, a more extensive investigation on unsupervised and supervised ML performance is recommended in future works. The supervised ML models such as neural networks, and fuzzy modelling could be a reasonable approach for identifying both the D_{50} and Q_s, by using the ADCP data as inputs. Moreover, physics-based variables used as inputs in the same models could also enhance efficiency. The cwt analysis should be applied for different bedload conditions and time sequences, to possibly establish a routine for more efficient filtering of the ADCP data, but also for automatic detection of gravel pulsations or bedload superimpositions, for which possibly longer measurements are advised. In addition, the cwt could deliver more features (i.e. peaking frequency) to be used as input variables in machine learning models.

5 Conclusions

The collected data by two different commercial ADCPs, in large navigable sand-gravel rivers, demonstrated a possibility to use the BS strength for detecting the median bedload grain size, as well as to indicate the bedload concentration (i.e. the active bedload layer). The B_s measured by the M9 – 0.5 MHz – gave the most consistent, almost linear and positive correlation with the D_{50}, because of the 90° grazing angle, and limited influence of the volume scattering initiated by the active bedload layer. It should be noted that the PSD of the immobile bed did not deviate significantly from mobile bed material (i.e. armoured layer vs. moving bedload), which contributed to a better performance of the vertical beam, M9. At the same time, for the M9 – 0.5 MHz, B_s resulted in a weak negative correlation when compared with the bedload intensity, possibly due to the surface deformation and insensitivity to volume scattering. On the other hand, the acoustic losses through the active bedload layer impacted the B_s of M9 – 3 MHz; which yielded a very poor correlation with the D_{50} and increasing trends for sand and gravel versus the corresponding bedload intensities. These results showed that the vertical beam represented a most useful complementary information, regardless of the steep slope of the linear regression line. Conversely, the 3 MHz beam set is sampling the top of the active layer resulting in biased backscatter data which is not directly related to PSD features.

The 1.2 MHz BS strength data showed parabolic behaviour, deviating from the Rayleigh regime (i.e. higher B_s values for coarser PSD corresponding to larger D_{50}), at the point of transition from sand to gravel. This was a coupled effect of the finer profiling resolution of the RDI and the scattering losses due to the rough immobile bed surface. The 1.2 MHz, again, was almost insensitive to the bedload transport conditions, reflecting the influence of surface scattering due to the finer echo profiling resolution and the coded BB signal processing. This phenomenon makes the B_s from the RDI – 1.2 MHz more suitable for grainsize identification, despite the slanted beams; however, this should be further examined with large range of PSDs and surface slopes.

The temporal analysis of a single measurement has demonstrated the importance of the correct averaging, identification of bedload pulsations, and possible detection of turbulent events (e.g. bursting, or low-streak pulsations) that induce bedload motion. Particularly relevant for result reliability, the temporal analysis enables data filtering from external disturbances, such as local waves from the nearby boats. This analysis separated flow and transversal direction by considering instrumental reference system almost aligned to those directions (i.e. acoustic beam pairs lying in two perpendicular vertical planes aligned and perpendicular to flow). This demonstrates that the apparent velocity in the flow direction (from the two beams lying in the vertical plane aligned to flow) better compares to bedload rate from samples whereas the other pair of beams frequently results in v_a degradation. This corroborates the need for accurate and firmly fixed ADCP deployment in the field and v_a filtering based on the angle deviation to corresponding water velocity from ADCP.

Coupling the v_a and B_s, by using an unsupervised machine learning approach indicated a possibility of classifying the bedload data related to their transport intensity and grain size. The clustering was most efficient for the M9 using both 3 MHz and 0.5 MHz, which, again, confirmed the importance of the vertical beam in the grain sizes classification. This somehow compensates for M9 – 3 MHz slanted beams' sensitivity to volume scattering. This method could be useful in cases where the physical measurements are lacking, and identification of the active bedload area is required.

Acknowledgements

The authors acknowledge the collaboration with Sontek Xylem, which allowed free use of the ADPviewer software permitting full control of the M9 ADCP. It should be mentioned that this software is not commercially available. The authors also acknowledge the help of the technical staff from the German national Waterways and Shipping Administration (WSV), giving their full support during the measurement campaigns.

Disclosure statement

No potential conflict of interest was reported by the author(s).

Funding

The MaHYD project was funded within the governmental research and development-budget of the Federal Ministry for Digital and Transport (BMDV), Germany.

Notation

A_f = area of the surface scattering at flume bed (dB)
ADCP = acoustic current Doppler profiler (–)
B_s = corrected backscattering strength (dB)
BS = backscattering (–)
BT = bottom track (–)
$C_{v_{va}}$ = coefficient of variation of the apparent bedload velocity (–)
$C_{v_{BS}}$ = coefficient of variation of the backscattering strength (–)
cwt = continuous wavelet transformation (–)
D_{50} = particle median diameter (m)
D_{90} = particle diameter bigger than 90% (m)
D_{std} = standard deviation of the PSD (m)
EI = BT echo intensity (dB)
E_r = noise level (dB)
f = ADCP working frequency MHz
FD = percentage of the discarded velocity samples after the filtering (%)
g = gravitational constant (m s^{-2})
GMM = Gaussian mixture models (–)
H = water depth (m)
IC = incoherent signal processing
P_{dB} = transmit voltage (dB)
Pl = acoustic pulse length (mm)
PSD = particle size distribution (–)
Q_s = physically measured transport rate at the end of the flume (kg s m^{-1})
R = slant distance from the transducer to the sediment bed (m)
S = slope of the river surface (%)
S_{L0} = source level (dB)
$std(va)$ = standard deviation of the raw apparent bedload velocity (m s^{-1})
S_s = surface backscattering (dB)
S_v = volume backscattering (dB)
std = standard deviation (–)
U = average-depth water velocity (m s^{-1})
$u*$ = shear(friction) velocity (m s^{-1})
v_a = the apparent velocity, measured by the ADCPs and filtered (m s^{-1})
v_{BT} = bottom tracking velocity (m s^{-1})
v_{gps} = GPS vessel velocity (m s^{-1})
α = attenuation coefficient (–)
λ = wavelength (mm)
φ = acoustic beam opening angle (°)
θ = acoustic beam incident angle (°)

References

Aleixo, M. G., Nones, M., & Ruther, N. (2020). Applying ADCPs for long term monitoring of SSC in rivers. *Water Resources Research*, *56*(1), 1–23. doi:10.1029/2019WR026087

Bagnold, R. (1956). The flow of cohesionless grains in fluids. *Philos. Trans. R. Soc. London*, *249*(A), 235–297. doi:10.1098/rsta.1956.0020

Banhold, K., Schüttrumpf, H., Hillebrand, G., & Frings, R. (2016). Underestimation of sand loads during bed-load measurements—a laboratory examination. *The International Conference On Fluvial Hydraulics (River Flow 2016)*, 1036–1041. doi:10.1201/9781315644479-165

Barrière, J., Oth, A., Hostache, R., & Krein, A. (2015). Bed load transport monitoring using seismic observations in a low-gradient rural gravel bed stream: Seismic monitoring of bedload transport. *Geophysical Research Letters*, *42*(7), 2294–2301. doi:10.1002/2015GL063630

Blanckaert, K., Heyman J, H., & Rennie, C. D. (2017). Measurments of bedload sediment transport with an Acoustic Doppler Velocity Profiler(ADVP). *J. Hydraulic Engineering*, *143*(6), doi:10.1061/(ASCE)HY.1943-7900.0001293

Brandstetter, B., Gehres, N., & Vollmer, S. (2012). *Messverfahren des Geschiebetriebs für Wasserstraßen. Bundesanstalt für Gewässerkunde*. BfG-1761.

Brumley, B. H., Cabrera, R. G., Deines, K. L., & Terray, E. A. (1991). Performance of a broad-band acoustic Doppler current profiler. *IEEE Journal of Oceanic Engineering*, *16*(4), 402–407. doi:10.1109/48.90905

Bunte, K., Swingle, K. W., & Abt, S. R. (2007). *Guidelines for using bedload traps in coarse-bedded mountain streams: Construction, installation, operation, and sample processing*. Gen. Tech. Rep. RMRS GTR-191., Fort Collins, CO:: U.S. Department of Agriculture, Forest Service.

Church, M., & Haschenburger, J. K. (2017). What is the "active layer"? *Water Resources Research*, *53*(1), 5–10. doi:10.1002/2016WR019675

Claude, N., Rodrigues, S., Bustillo, V., Bréhéret, J., Macaire, J., & Jugé, P. (2012). Estimating bedload transport in a large sand–gravel bed river from direct sampling, dune tracking and empirical formulas. *Geomorphology*, *179*, 40–57. doi:10.1016/j.geomorph.2012.07.030

Conevski, S., Aleixo, R., Guerrero, M., & Ruther, N. (2020c). Bedload Velocity and Backscattering Strength from Mobile Sediment Bed: A Laboratory Investigation Comparing

Bistatic Versus Monostatic Acoustic Configuration. *Water*, *12*(12), 3318. doi:10.3390/w12123318

Conevski, S., Guerrero, M., Colin, R., & Ruther, N. (2020a). Acoustic sampling effects on bedload quantification using acoustic Doppler current profilers. *Journal of Hydraulic Research*, *58*(6), 982–1000. doi:10.1080/00221686.2019.1703047

Conevski, S., Guerrero, M., Rennie, C., & Ruther, N. (2020b). Towards an evaluation of bedload transport characteristics by using doppler and backscatter outputs from ADCPs. *Journal of Hydraulic Research*, *59*, 703–723. doi:10.1080/00221686.2020.1818311

Conevski, S., Guerrero, M., Ruther, N., & Rennie, C. (2019). Laboratory Investigation of Apparent Bedload Velocity Measured by ADCPs under Different Transport Conditions. *Journal of Hydraulic Engineering*, *145*. doi:10.1061/(ASCE)HY.1943-7900.0001632

Conevski, S., Guerrero, M., Winterscheid, A., & Ruther, N. (2022). Comprehensive Analysis of the Bottom Tracking features measured by ADCPs in Riverine Environments. *Redigert av Miguel Ortega-Sánchez. Granada: IAHR*, 814–823. doi:10.3850/IAHR-39WC2521711920221921

Conevski, S., Winterscheid, A., Ruther, N., Guerrero, M., & Rennie, o. C. (2018). «Evaluation of an acoustic Doppler technique for bed-load transport measurements in sand-bed rivers.» *River Flow 2018*. Lyon: Paper presented at River Flow 2018.

Darrell, R. J., & Richardson, M. D. (2007). *High-Frequency Seafloor Acoustics*. Springer Science + Business Media, LLC.

Foufoula-Georgiou, E., & Kumar, P. (1994). *Wavelet analysis and its applications*. Redigert av CHARLES K. CHUI. Academic Press, Inc. 1–43. ISBN 0-12-262850-0.

Frings, R. M., & Stefan, V. (2017). Guidelines for sampling bedload transport with minimum uncertainty. *Sedimentology*, *64*(6), 1630–1645. doi:10.1111/sed.12366

Gaeuman, D., & Jacobson, R. B. (2006). Acoustic bed velocity and bed load dynamics in a large sand bed river. *Journal of Geophysical Research*, *111*(F2), F02005. doi:10.1029/2005JF000411

Gaweesh, M., & Van Rijn, L. (1994). Bed-Load Sampling in Sand-Bed Rivers. *Journal of Hydraulic Engineering*, *120*(12), 1364–1384. doi:10.1061/(ASCE)0733-9429(1994)120:12(1364)

Geay, T., Belleudy, P., Gervaise, C., Habersack, H., Aigner, J., Kreisler, A., Seitz, H., & Laronne, J. B. (2017). Passive acoustic monitoring of bed load discharge in a large gravel bed river. *Journal of Geophysical Research: Earth Surface*, *122*(2), 528–545. doi:10.1002/2016JF004112

Gomez, B. (1991). Bedload transport. *Earth-Science Reviews*, *31*(2), 89–132. doi:https://doi.org/10.10160012-8252(91)90017-A

Guerrero, M., Rüther, N., Szupiany, R., Haun, S., Baranya, S., & Latosinski, F. (2016). The acoustic properties of suspended sediment in large rivers: Consequences on ADCP methods applicability. *Water (Switzerland) (MDPI AG*, *8*(1), 13. doi:10.3390/w8010013

Guerrero, M., Szupiany, R., & Latosinski, F. (2013). Multifrequency acoustics for suspended sediment studies: an application in the Parana River. *Journal of Hydraulic Research*, *51*(6), 696–707. doi:10.1080/00221686.2013.849296

Guta, H., Hurther, D., & Chauchat, J. (2022). Bedload and Concentration Effects on Turbulent Suspension Properties in Heavy Particle Sheet Flows. *Journal of Hydraulic Engineering*, *148*(7), 04022012. doi:10.1061/(ASCE)HY.1943-7900.0001988

Haun, S., Rüther, N., Baranya, S., & Guerrero, M. (2015). Comparison of real time suspended sediment transport measurements in river environment by LISST instruments in stationary and moving operation mode. *Flow Measurement and Instrumentation*, *41*, 10–17. doi:10.1016/j.flowmeasinst.2014.10.009

Hsu, L., Finnegan, N. J., & Brodsky, E. E. (2011). A seismic signature of river bedload transport during storm events. *Geophysical Research Letters*, *38*. https://doi.org/10.1029/2011GL047759

Hubbell, D. W. (1964). *Apparatus and techniques for measuring bedload*. USGS, U. S. Govt. Print. Off. doi:10.3133/wsp1748.

Hurther, D., & Thorne, P. D. (2011). Suspension and near-bed load sediment transport processes above a migrating, sand-rippled bed under shoaling waves. *Journal of Geophysical Research: Oceans*, *116*. doi:10.1029/2010JC006774

Ivakin, A. N. (1981). Underwater sound scattering by volume inhomogeneities of a bottom medium bounded by a rough surface. *Soviet Physics Acoustics*, *27*(3), 212–215.

Jamieson, E. C., Rennie, C. D., Jacobson, R. B., & Townsend, R. D. (2011). Evaluation of ADCP apparent bed load velocity in a large sand-bed river: Moving versus stationary boat conditions. *Journal of Hydraulic Engineering*, *137*(9), 1064–1071. doi:10.1061/(ASCE)HY.1943-7900.0000373

Jamieson, E., Rennie, C. D., & Ramooz, R. (2008). Verification of in-situ ADCP bedload transport measurements using digital video analysis. *River Flow 2008, IHAR*.

Jothilakshmi, S., & Gudivada, V. N. (2016). Chapter 10 – large scale data enabled evolution of spoken language research and applications. I *Handbook of Statistics*, redigert av Venkat N. Gudivada, Venkat N. Raghavan and C.R. Rao, Venu Govindaraju, 301–340. Elsevier. doi:10.1016/bs.host.2016.07.005.

Le Guern, J., Rodrigues, S., Geay, T., Zanker, S., Hauet, A., Tassi, P., Claude, N., Jugé, P., Duperray, A., & Vervynck, L. (2021). Relevance of acoustic methods to quantify

bedload transport and bedform dynamics in a large sandy-gravel-bed river. *Earth Surface Dynamics*, *9*(3), 423–444. doi:10.5194/esurf-9-423-2021

Leary, K., & Buscombe, D. (2020). Estimating sand bed load in rivers by tracking dunes: a comparison of methods based on bed elevation time series. *Earth Surface Dynamics*, *8*(1), 161–172. doi:10.5194/esurf-8-161-2020

Lee Gordon, R., & Instruments, R. D. (1996). *Acoustic doppler current profiler principles of operation a practical primer*. San Diego, CA: RD Instruments.

Lilly, J. M. (2017). Element analysis: a wavelet-based method for analysing time-localized events in noisy time series. *Proceedings of the Royal Society A: Mathematical, Physical and Engineering Sciences*, *473*(2200). doi:10.1098/rspa.2016.0776

Medwin, H. (2005). *Sounds in the sea: From ocean acoustics to acoustical oceanography*. Cambridge University Press.

Medwin, H., & Clay, C. S. (1998). *Fundamentals of acoustical oceanography*. Academic Press.

Moate, B. D., & Thorne, P. D. (2009). Measurements and inversion of acoustic scattering from suspensions having broad size distributions. *The Journal of the Acoustical Society of America*, *126*(6), 2905–2917. doi:10.1121/1.3242374

Moore, S. A., Dramais, G., Dussouillez, P., Le Coz, J., Rennie, C., & Camenen, B. (2013). Acoustic measurements of the spatial distribution of suspended sediment at a site on the Lower Mekong River. *Proceedings of Meetings on Acoustics*, *19*, 005003. doi:10.1121/1.4799128

Moore, S. A., Le Coz, J., Hurther, D., & Paquier, A. (2012). On the application of horizontal ADCPs to suspended sediment transport surveys in rivers. *Continental Shelf Research*, *46*, 50–63. doi:10.1016/j.csr.2011.10.013

Muste, M., Baranya, S., Tsubaki, R., Kim, D., Ho, H., Tsai, H., & Law, D. (2016). Acoustic mapping velocimetry. *Water Resources Research*, *52*(5), 4132–4150. doi:10.1002/2015WR018354

Nezu, I., & Nakagawa, H. (1993). *Turbulence in open channel flows. IAHR monograph*. A. A. Balkema.

Parker, G. (2004). *ID sediment transport morphodynamics with applications to rivers and turbidity currents*. St. Anthony Falls Laboratory, Mississippi River at 3rd Avenue SE.

RDInstruments. (2011). Acoustic doppler current profiler principles of operation a practical primer. Practical Primer, Teledyne RD Instruments, 14020 Stowe Drive Poway, California 92064. http://www.teledynemarine.com.

RDInstruments, Teledyne. (2015). *StreamPro ADCP Guide.* Teledyne RDInstruments. http://www.teledynemarine.com/Documents/Brand%20Support/RD%20INSTRUMENTS/Technical%20Resources/Manuals%20and%20Guides/StreamPro/StreamPro_ADCP_Guide_Sep15.pdf.

Rennie, C. D., & Church, M. (2010). Mapping spatial distributions and uncertainty of water and sediment. *Journal of Geophysical Research-Earth Surface*, *115*, F03035. doi:10.1029/2009JF001556, 2010

Rennie, C. D., & Millar, R. (2007). Deconvolution technique to separate signal from noise in gravel bedload velocity data. *Journal of Hydraulic Engineering-Asce*, *8*(8), 845–856. doi:10.1061/(ASCE)0733-9429(2007)133:8(845)

Rennie, C. D., Millar, R. G., & Church, M. A. (2002). Measurement of bed load velocity using an acoustic doppler current profiler. *Journal of Hydraulic Engineering*, *128*(5), 473–483. doi:10.1061/(ASCE)0733-9429(2002)128:5(473)

Rennie, C. D.,Vericat, D., Williams, R. D., Brasington, J., & Hicks, M. (2017). Calibration of acoustic doppler current profiler apparent bedload velocity to bedload transport rate. Kap. 8 i *Gravel-Bed Rivers: Process and Disasters*, 209–231. Wiley-Blackwell.

Rennie, C. D., & Villard, P. V. (2004). Site specificity of bed load measurement using an acoustic Doppler current profiler. *Journal of Geophysical Research: Earth Surface*, *109*. doi:10.1029/2003JF000106

Rickenmann, D., Turowski, J. M., Fritschi, B., Klaiber, A., & Ludwig, A. (2012). Bedload transport measurements at the Erlenbach stream with geophones and automated basket samplers. *Earth Surface Processes and Landforms*, *37*(9), 1000–1011. doi:10.1002/esp.3225

Rickenmann, D.,Turowski, J. M., Fritschi, B., Wyss, C., Laronne, J., Barzilai, R., Reid, I. (2014). Bedload transport measurements with impact plate geophones: comparison of sensor calibration in different gravel-bed streams. *Earth Surface Processes and Landforms*, *39*, 928–942. doi:10.1002/esp.3499

Roth, D., Brodsky, E., Finnegan, N., Rickenmann, D., Turowski, J., & Badoux, A. (2016). Bed load sediment transport inferred from seismic signals near a river. *Journal of Geophysical Research: Earth Surface*, *121*(4), 725–747. doi:10.1002/2015JF003782

Shields, D. F. Jr. (2010). Aquatic habitat bottom classification using ADCP. *Journal of Hydraulic Engineering*, *136*, 336–342. doi:10.1061/(ASCE)HY.1943-7900.0000181

Simons, D. B., Richardson, E. V., & Nordin, C. F. (1965). *Bedload equation for ripples and dunes*. US Government Printing Office.

Sontek. (2017). *RiverSurveyor S5/M9 system manual, firmware version 4.02.* 9940 Summers Ridge Road, San Diego, CA 92121-3091 USA: SonTek, a Xylem brand. http://ysi.actonsoftware.com/acton/attachment/1253/f-041f/1/-/-/-/-/RiverSurveyor%20Live%20Manual%20v4.0_R.pdf.

Szupiany, R. N., Weibel, C. L., Guerrero, M., Latosinski, F., Wood, M., Ruben, L. D., & Oberg, K. (2019). Estimating sand concentrations using ADCP-based acoustic inversion in a large fluvial system characterized by bi-modal

suspended-sediment distributions. *Earth Surface Processes and Landforms*, *44*(6), 1295–1308. doi:10.1002/esp.4572

Thorne, P. D., & Hurther, D. (2014). An overview on the use of backscattered sound for measuring suspended particle size and concentration profiles in non-cohesive inorganic sediment transport studies. *Continental Shelf Research*, *73*, 97–118. doi:10.1016/j.csr.2013.10.017

Urick, R. J. (1983). *Principles of underwater sound*. Peninsula Publishing. https://books.google.no/books?id=MBBgQgAACAAJ.

Van Rijn, L. (1984). Sediment transport, part i: Bed load transport. *Journal of Hydraulic Engineering*, *110*(10), 1431–1456. doi:10.1061/(ASCE)0733-9429(1984)110:10(1431)

Vries, D. (1979). *Information on the Arnhem Sampler (BTMA)*. Internal Report No. 3-79, Delöft University of Technology,, Delöft : Delöft University of Technology.

Wilcock, P., Pitlick, J., & Cui, Y. (2009). *Sediment transport primer – Estimating bed-material transport in gravel-bed rivers*. Rocky Mountain Research Station, U.S. Department of Agriculture, Forest Service, Gen. Tech. Rep. RMRS-GTR-226. Fort Collins, CO.